JACS
JOURNAL OF THE AMERICAN CHEMICAL SOCIETY
Article
pubs.acs.org/JACS

The Impact of Antiaromatic Subunits in [4*n*+2] π-Systems: Bispentalenes with [4*n*+2] π-Electron Perimeters and Antiaromatic Character

Jing Cao,[†,∥] Gábor London,[†,⊥,∥] Oliver Dumele,[†,∥] Margarete von Wantoch Rekowski,[†] Nils Trapp,[†] Laurent Ruhlmann,[‡] Corinne Boudon,[‡] Amnon Stanger,*[,§] and François Diederich*[,†]

[†]Laboratory of Organic Chemistry, ETH Zurich, Vladimir-Prelog-Weg 3, CH-8093 Zurich, Switzerland

[‡]Laboratoire d'Electrochimie et de Chimie Physique du Corps Solide, Institut de Chimie-UMR 7177, C.N.R.S., Université de Strasbourg, 4 rue Blaise Pascal, 67081 Strasbourg Cedex, France

[§]Schulich Faculty of Chemistry and the Lise Meitner-Minerva Center for Computational Quantum Chemistry, Technion-Israel Institute of Technology, Haifa, 3200008, Israel

Supporting Information

ABSTRACT: Three series of stable, neutral, π-extended bispentalene derivatives, with two pentalenes fused to a central benzene or naphthalene moiety, have been prepared through a modified double carbopalladation cascade reaction. While these chromophores feature skeletons with [4*n*+2] π-electron perimeters, the two 8 π-electron pentalene subunits strongly influence bonding and spectral properties. ^{1}H NMR spectra showed large upfield shifts of the protons in the pentalene moieties, comparable to antiaromatic monobenzopentalenes. Further investigations on magnetic ring currents through NICS-XY-scans suggest a global paratropic current and a local diatropic current at the central benzene ring in two of the series, while the third series, with a central naphthalene ring, showed more localized ring currents, with stronger paratropic ring currents on the pentalene moieties. X-ray diffraction analyses revealed planar bispentalene cores with large double- and single-bond alternation in the pentalene units, characteristic for antiaromaticity, and small alternation in the central aromatic rings. In agreement with TD-DFT calculations, both optical and electrochemical data showed much smaller HOMO−LUMO energy gaps compared to other neutral, acene-like hydrocarbons with the same number of fused rings. Both experimental and computational results suggest that the molecular properties of the presented bispentalenes are dominated by the antiaromatic pentalene-subunits despite the [4*n*+2] π-electron perimeter of the skeletons.

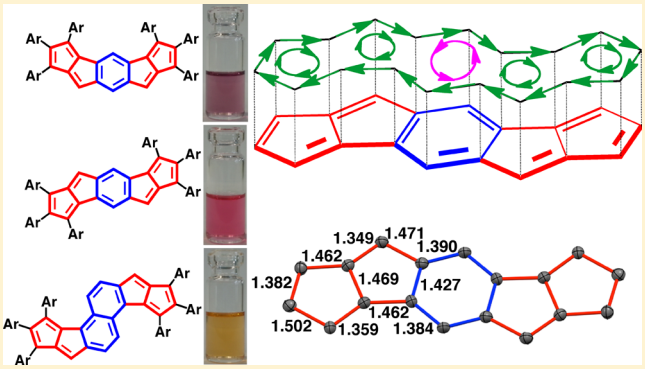

INTRODUCTION

The concepts of aromaticity and antiaromaticity are of fundamental importance in classifying physical and chemical properties of planar, π-conjugated cyclic molecules.[1] According to Hückel's rule,[2] planar, π-conjugated monocyclic systems with [4*n*+2] π-electrons exhibit conjugative stabilization in the ground state and are called aromatic compounds. Later, Frost and Musulin,[3] and Breslow[4] extended Hückel's work and introduced the term antiaromaticity to describe conjugated cyclic systems whose π-electron energy is higher than that of a suitable reference compound, which is not cyclically delocalized.[4] A series of intuitively acceptable criteria for aromaticity and antiaromaticity of neutral, even-electron singlet species were thus established by Breslow and summarized by Krygowski et al.[1c,5] These criteria describe aromaticity and antiaromaticity from six different aspects, including electronic nature, energy, geometry, magnetic properties, reactivity, and spectroscopic properties. However, until now, no unique definition for aromaticity and antiaromaticity is generally accepted.[1,6] Additionally, theoretical studies[7] suggest that the aromaticity (or antiaromaticity) of neutral, π-conjugated polycyclic hydrocarbons should be determined by the number of conjugated π-electrons as well as by the nature of their fragmental structures. Therefore, investigations on the electronic structures, physical properties, and chemical reactivity of π-conjugated polycyclic systems with [4*n*+2] π-electron perimeter containing antiaromatic-subunits, which make a dominant contribution to the overall properties, are of special interest, although experimentally rare.[8]

Nowadays, polycyclic aromatic hydrocarbons (PAH) are attracting tremendous interest as advanced materials.[9,10] Especially studied are linear acenes, such as pentacene and derivatives,[10] because of their planar conjugated structures and

Received: March 28, 2015
Published: May 15, 2015

DOI: 10.1021/jacs.5b03074
J. Am. Chem. Soc. 2015, 137, 7178−7188

fascinating optical and electronic properties that have great potential in organic electronics. However, insufficiently substituted acenes are prone to oxidation and dimerization under ambient conditions.[10b,11] Thus, research toward alternative, acene-like structures earns increasing attention. Investigations show that the combination of extended π-conjugation and proper lowering of aromaticity within the same scaffold is an effective way to achieve high charge mobilities in fused ring systems.[10b] Furthermore, theoretical predictions indicate the high performance of antiaromatic rings in electrical conductivity.[12] Apart from the widely used methods of replacing benzene rings in acenes by heteroaromatic rings[13] to lower aromaticity,[10b] another recently developed important strategy is the incorporation of nonhexagonal hydrocarbon rings into the acene framework.[14,15] In this regard, fully π-conjugated indenofluorene derivatives[15] (e.g., Figure 1a,b) with

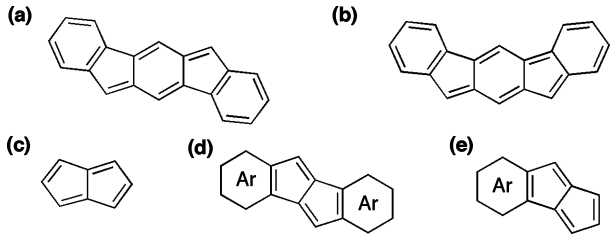

Figure 1. Structures of (a) indeno[1,2-*b*]fluorene, (b) indeno[2,1-*b*]fluorene, (c) pentalene, (d) bisannulated[*a*,*e*]pentalene, (e) monoannulated pentalene.

a 6−5−6−5−6 fused ring system that possess an overall 4*n* π-electronic structure have recently received particular attention. Within that class, especially promising candidates are the indeno[1,2-*b*]fluorene and indeno[2,1-*b*]fluorene derivatives (Figure 1a,b), as they exhibit ambipolar carrier transportation properties both in single-crystal organic field-effect transistors (OFETs)[15b] and in thin-film OFETs.[15c] However, acene-like π-conjugated polycyclic hydrocarbons containing more than two cyclopentadiene rings, have rarely been explored.[16]

Pentalene (Figure 1c) is a fully antiaromatic compound[7d] consisting of two fused cyclopentadiene rings with 8 π electrons.[17] It dimerizes above −196 °C without electronic or steric stabilization of the core.[18] Major recent synthetic advances, with focus on bisannulated[*a*,*e*]pentalene derivatives (Figure 1d), include the transition metal-mediated annulation,[16b,19] $B(C_6F_5)_3$-induced intramolecular coupling,[20] and anionic or radical anionic trans-annulation.[21] Dinaphtho[*a*,*e*]-pentalene thin films[19a,f,g] and dibenzopentalene (DBP)-based conjugated polymers[22] showed high charge mobilities, being potential candidates for organic/polymeric thin-film transistors.

Recently, our group developed a simple and rapid method toward monoannulated pentalene derivatives (Figure 1e), based on a cascade carbopalladation reaction between *gem*-dibromoolefins and alkynes.[23] This methodology provides access to extended polycyclic hydrocarbons with pentalene moieties. Herein, we report the synthesis of bispentalene derivatives **1**−**3** (Figure 2) with different fusion patterns and functional groups through a double cascade carbopalladation reaction between the corresponding bis(*gem*-dibromoolefins) and alkynes involving the formation of six C−C bonds during the one-pot reaction. Structurally, bispentalenes **1**−**2** consist of four cyclopentadiene subunits replacing four of the benzene rings in the parent pentacene structure, as compared to two cyclopentadiene rings in indenofluorene derivatives (Figure 1a,b).[14,15] The structure and physicochemical properties of the synthesized compounds **1**−**3** were characterized by means of NMR spectroscopy, nucleus-independent chemical shift (NICS)-XY-scan,[24] X-ray crystallographic analysis, UV−vis spectroscopy, and electrochemistry. The obtained data are indicative of the antiaromatic nature of the bispentalene core despite the [4*n*+2] π-electron perimeter of the molecules.

RESULTS AND DISCUSSION

Synthesis. The key steps toward bispentalene derivatives **1**−**3** are outlined in Scheme 1. Bis(*gem*-dibromoolefin) derivatives **4**, **6**, and **7** were prepared by the Ramirez olefination reaction[25] starting from the corresponding dialdehydes (for complete synthetic details, see Section S2, Supporting Information). When bis(*gem*-dibromoolefin) **4** was first treated under the standard cascade carbopalladation reaction conditions established in our initial work,[23a] 90% of it was recovered and only traces of the desired product **1a** were detected by mass spectrometry and ^{1}H NMR spectroscopy.

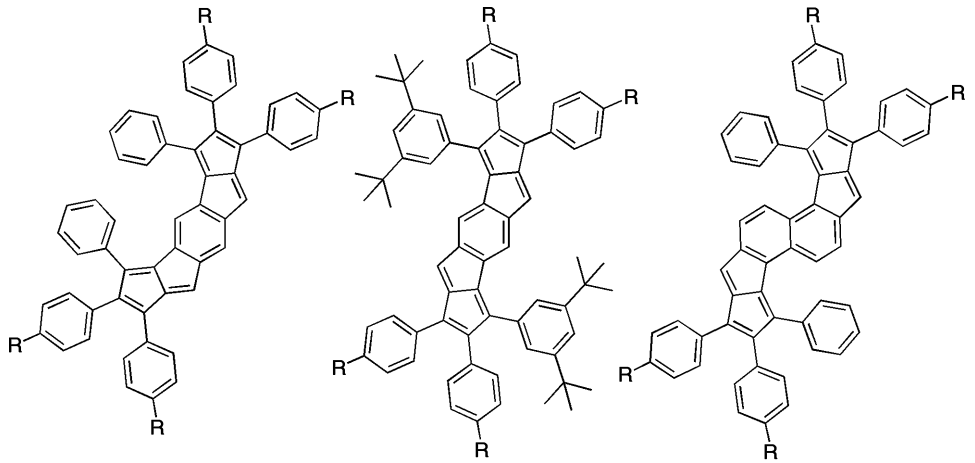

Figure 2. Structures of extended bispentalene derivatives **1**−**3**.

DOI: 10.1021/jacs.5b03074
J. Am. Chem. Soc. 2015, 137, 7178−7188

Scheme 1. Key Steps Towards Bispentalene Derivatives 1−3[a]

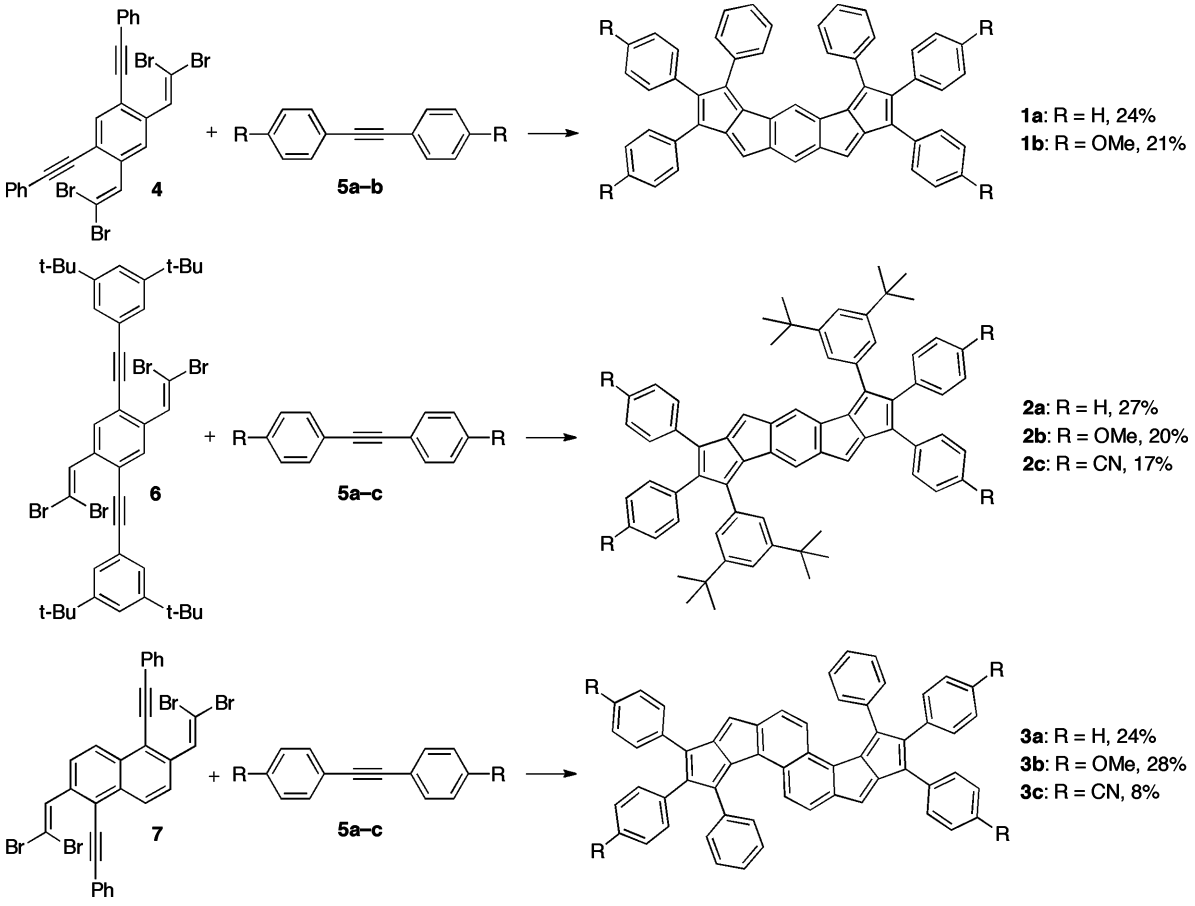

[a]Reaction conditions: alkyne **5** (6.0 equiv), $[Pd(PPh_3)_2Cl_2]$ (0.2 equiv), K_2CO_3 (4.0 equiv), Zn dust (2.0 equiv), hydroquinone (4.0 equiv, added after heating 1−2 h at 110 °C), toluene, 110 °C, total heating time: 25−26 h.

Extension of the reaction time as well as addition of up to 1.0 equiv of palladium "catalyst" only enhanced the formation of unidentified byproducts. Furthermore, due to the large excess of the acetylene reagents and limited solubility of **1a**, further purification was deemed unfeasible.

The use of hydroquinone in the reaction turned out to be as effective as we found in our more recent studies.[23b] Not only could bispentalene **1a** be obtained in a reasonable yield of 24% with the formation of six new C−C bond in a one-pot cascade reaction, but also the amount of acetylene reagent could be decreased from 40 equiv to 6 equiv, which substantially facilitates the purification process. Prominently, hydroquinone was found beneficial only when it was added after the reaction mixture had been stirred at 110 °C for 1−2 h, but its exact role remains unknown. The reaction conditions shown in Scheme 1 were used for the preparation of all three series of compounds. Bispentalene derivative **1a** exhibited limited solubility in common solvents except for CS_2, which was subsequently used in both chromatographic purification and structural characterization. Double cascade carbopalladation reaction of bis(*gem*-dibromoolefin) **4** with 1,2-bis(4-methoxyphenyl)-ethyne **5b** was performed to improve the solubility through introduction of methoxy-substituents on the peripheral phenyl rings. Compound **1b** was obtained as a black solid that showed good solubility in common organic solvents such as CH_2Cl_2 and $CHCl_3$.

The reaction of bis(*gem*-dibromoolefin) **6** with three different diphenylacetylenes **5a−c** provided the three bispentalene derivatives **2a−c** as dark purple solids in moderate yields (Scheme 1). This series shows excellent solubility in common organic solvents, such as CH_2Cl_2 and $CHCl_3$, and methoxy-substituted **2b** could even dissolve in apolar hexane. Cyano-substituted **2c** is the least soluble of the three compounds.

To further extend the π-system, naphtho-fused bispentalene derivatives **3a−c** with 5−5−6−6−5−5 ring patterns were also prepared by reacting acetylenes **5a−c** with bis(*gem*-dibromoolefin) **7**. While methoxy-substituted **3b** showed the highest solubility in common organic solvents, the comparably poor solubility of cyano-substituted **3c** rendered its purification difficult, which lead to its low yield of 8%.

The molecular structures of **1a,b** and **2a−c** with 18 π-electrons and **3a−c** with 22 π-electrons in their perimeters were fully characterized by high-resolution mass spectrometry (HR-MS), ^1H NMR and ^{13}C NMR spectroscopy, and X-ray crystallography (see below). Their aromatic (or antiaromatic) properties were investigated through four aspects: magnetic properties, geometry, spectroscopic properties, and energy.[1c,5]

Thermal Stability of the Bispentalenes. Compounds **1−3** are deeply colored solids, which show high stability in the solid state at 298 K, with no obvious degradation even when exposed to air and light for months. Bispentalene **2a** is even thermally stable up to its melting point (295 °C) under

DOI: 10.1021/jacs.5b03074
J. Am. Chem. Soc. 2015, 137, 7178−7188

ambient conditions, while **1a**,**b**, **2c**, and **3c** completely decompose when heating up to 250 °C.

The relative stability of **1a**,**b**, **2a**,**b**, and **3a**,**b** in solution was examined by UV−vis spectroscopy under reported conditions,[11d] by monitoring the strongest absorption in the Vis region (for details, see Section S4, Supporting Information). Molecules **3a**,**b** degraded faster than the corresponding compounds from the other two series, with half-lives ($t_{1/2}$) of 50 and 20 h for **3a** and **3b**, respectively. This is likely due to the more electronically isolated nature of the antiaromatic pentalene and aromatic naphthalene units within compounds **3a**,**b**, as discussed below. Furthermore, the electron-donating methoxy substituents reduced the stability in solution, in agreement with the comparably high HOMO energy levels of these compounds (see below). Among the bispentalenes presented, **2a** showed the highest thermodynamic stability with no obvious degradation observed even after 2 weeks. This result indicates that introduction of bulky substituents is beneficial in both increasing the solubility and enhancing the stability of the bispentalene core.

^{1}H NMR Spectroscopy. It is widely accepted that aromatic systems have the ability to sustain a diatropic circulation of ring current in the presence of an external magnetic field.[1] In contrast, antiaromatic compounds sustain paratropic ring currents.[26] As a result, planar, cyclic conjugated π-electron systems exhibit specific magnetic properties that have reflections on ^{1}H NMR chemical shifts, magnetic susceptibility exaltation,[27] and nucleus-independent chemical shifts (NICS),[28] besides others.[1c]

In the ^{1}H NMR spectra of **1**−**3**, protons of the fused bispentalene chromophores appeared significantly upfield compared to those of the peripheral phenyl substituents. As shown in Figure 3, the proton signals of H1 in the cyclopentadiene rings of **1**−**3** appear in the region between 5.80−6.05 ppm, whereas the same proton in monobenzopentalene **S9** bearing the same two 4-methoxyphenyl substituents is located at about 6.29 ppm (Figure S28, Supporting Information). The upfield shift of the protons in the central benzene ring of **2b** (H2, Figure 3b) is even larger than those of the protons in 6,12-diaryl substituted indeno[1,2-*b*]fluorenes, 20 π-electron molecules, by about 0.70 ppm.[15b] There are clearly pronounced ring current effects in bispentalenes **1**−**3**; however, the contribution of electronic substituent effects and shielding/deshielding effects from the peripheral phenyl ring cannot be neglected for specific protons at the annellated core.

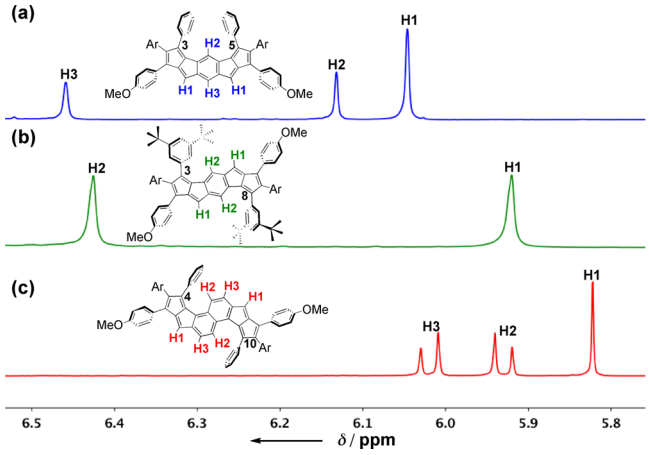

Figure 3. Partial ^{1}H NMR spectra (400 MHz, $CDCl_3$, 298 K) of compound (a) **1b**, (b) **2b**, and (c) **3b**.

Comparison of the proton signals in the central six-membered rings of **1b**, **2b**, and **3b** sheds light on these multiple effects. For instance, in compound **3b**, the chemical shifts of the naphthalene protons appear at δ = 5.93 (H2) and 6.02 (H3) ppm (Figure 3c) in $CDCl_3$ at 298 K. While in benzo-fused bispentalene **2b**, the corresponding signals are located at δ = 6.43 (H2) ppm (Figure 3b). One possibility for this difference might be the different ring current effects. Notably, all three protons are situated in the shielding regions of the peripheral phenyl substituents (on C(3), C(8) in **2b**; on C(4), C(10) in **3b**, Figure 3). The dihedral angle between the plane of these phenyl rings and the central core is only relevant if the hydrogen atoms are in close proximity to the peripheral phenyl rings: in this case, the more perpendicular the two planes are, the stronger the shielding effect. The distances between the protons and peripheral phenyl ring could not be neglected either. In compound **1b** (Figure 3a), the larger upfield shift of H2 (δ = 6.13 ppm), compared to H3 (δ = 6.46 ppm), could be attributed to the shielding effects from the two proximal phenyl rings (on C(3) and C(5), Figure 3a). However, although no shielding effect comes from the phenyl substituents, the proton signal of H3 in **1b** is still shifted upfield with respect to the normal aromatic region.

Bispentalene derivatives **2a**−**c** (Figure S40, Supporting Information) showed no significant effects of the substituents at the peripheral phenyl rings on the chemical shifts. We therefore conclude that the major part of the magnetic shielding effects observed in **1**−**3** originates from induced ring currents in the fused bispentalene chromophores.

NICS-XY-Scans. Complementary to ^{1}H NMR spectroscopy, NICS-based methods[28] are more convincing and widely used for the identification of induced ring currents within π-conjugated cyclic systems. Negative NICS values are denoted to induced diatropic ring currents, while positive values are indicative of paratropic ring currents.[28a]

Since bispentalenes **1**−**3** are π-conjugated polycyclic hydrocarbons, their aromatic (or antiaromatic) properties cannot be understood by looking at individual rings. Thus, the magnetic shielding properties of compounds **1**−**3** were investigated by the recently established NICS-XY-scan, which can explore the types of ring currents (namely, diatropic, paratropic, global, and local) in π-conjugated polycyclic systems.[24] A global ring current refers to the current for the entire molecule, while a local ring current describes the induced current circuit at a specific reference point in and near a molecule.[24,29] Existence of a global current only results in a flat NICS-XY-scan above the molecule (see, for example naphthalene[24]), while the coexistence of global, semiglobal and local current results in a nonflat curve (see, for example, anthracene[24]).

The NICS-XY-scan of pentalene serves as a reference: a global pentalenic paratropic current (Figure 4a) of ca. 24 ppm[30] and two local, relatively small (ca. 3 ppm) paratropic currents at each five-membered ring were obtained. As seen in Figure 4b, the paratropic ring current of **1a** at the pentalene units is reduced (ca. 11 ppm vs 24 ppm in pentalene), while at the central benzene ring there is a small paratropic current (ca. 3 ppm), very different from benzene[24] (ca. −16 ppm). This suggests a global paratropic current for the 18 π-electron perimeter of 11 ppm and a local diatropic current at the six-membered ring of ca. −8 ppm (Figure 5). But we still could not neglect the semiglobal currents at the 5−5−6 membered ring

DOI: 10.1021/jacs.5b03074
J. Am. Chem. Soc. 2015, 137, 7178−7188

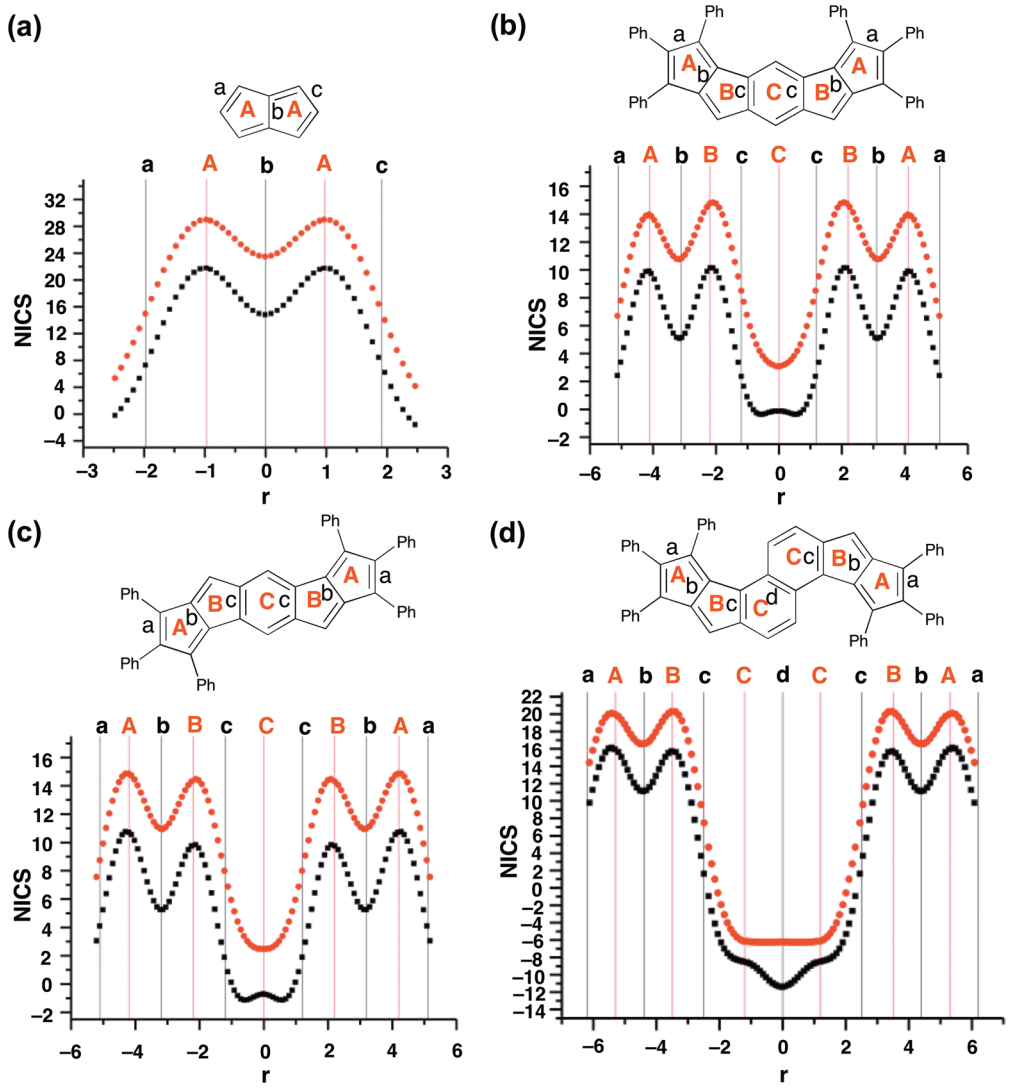

Figure 4. NICS-XY-scans of (a) pentalene, (b) bispentalene **1a**, (c) bispentalene **2d**, and (d) bispentalene **3a**. Black: $NICS_{ZZ}$. Red: $NICS_{\pi,ZZ}$.

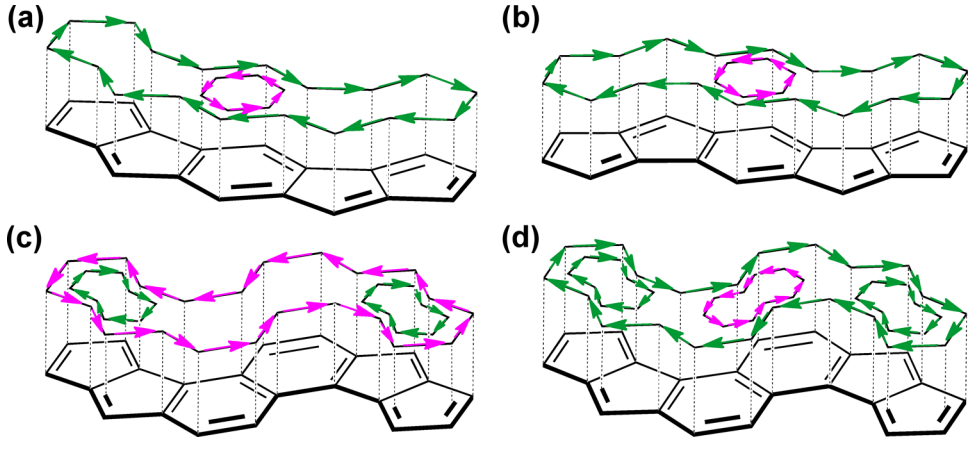

Figure 5. Scheme of induced ring currents from NICS-XY-scan results for (a) bispentalene **1**, (b) bispentalene **2**, (c) one possibility for bispentalene **3**, and (d) the second possibility for bispentalene **3**. Substituents and the small local paratropic currents at the five-membered rings (Figure S45, Supporting Information) are omitted for clarity.

subunits. However, even if these currents exist, the picture of global paratropic currents in the systems remains the same (for further details, see Section S6.2, Supporting Information). Thus, after fusion, both the paratropic ring current of the pentalene moieties and the diatropic ring current of the benzene unit in **1a** are reduced by ca. 50%.

Since the substituents on the peripheral phenyl rings in **2a** have a negligible effect on the induced ring currents of the

DOI: 10.1021/jacs.5b03074
J. Am. Chem. Soc. 2015, 137, 7178−7188

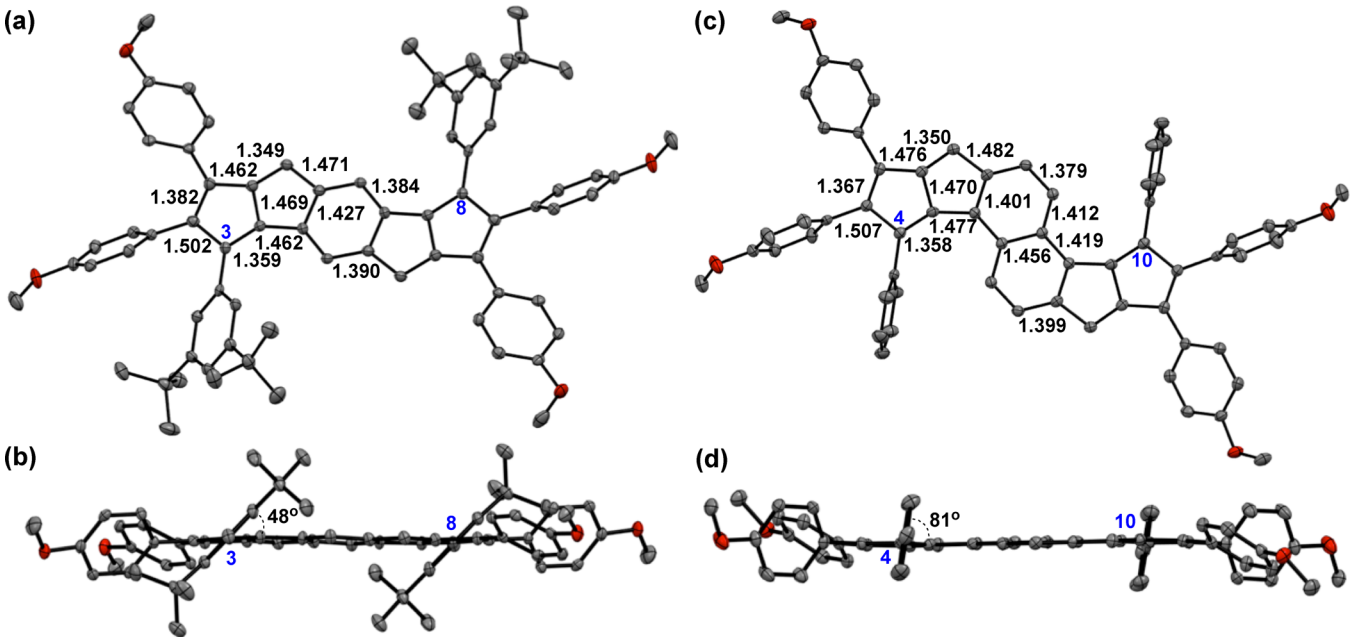

Figure 6. X-ray structures of (a) top view and (b) side view of **2b**; (c) top view and (d) side view of **3b**. Solvent molecules and hydrogen atoms are omitted for clarity. Compound **2b** and **3b** are C_{2h}-symmetric molecules with space group $P2_1/c$; only half of the bond lengths are presented. Thermal ellipsoids are drawn at 50% probability level at 100 K.

system (Table S1, Supporting Information), an analogue compound, **2d**, without *tert*-butyl groups was employed for calculation. Compound **2d** (Figure 4c) shows a very similar NICS-XY-scan to bispentalene **1a** (Figure 4b vs 4c), both the shape of the curves and the values are nearly the same. Moreover, the NICS(1)$_{\pi,ZZ}$ values, which report the magnetic environment above each ring (Table S1, Supporting Information), are almost identical in **1a** and **2d**. It is thus concluded that the magnetic properties of **1** and **2** are very similar, regardless of their different topologies (fused at the same sites).

The NICS-XY-scan of bispentalene **3a** shows NICS$_{\pi,ZZ}$ values of 17 ppm above the pentalene unit, while above the naphthalenic moiety the curve is constantly flat with a value of −6 ppm (Figure 4d). There are two plausible interpretations for the computed curves and values. One possibility is a 22 π-electron global diatropic current of −6 ppm and a "semi-local" paratropic current at the pentalenes of 23 ppm. The second possibility is a relatively weak global paratropic current and "semi-local" diatropic and paratropic currents at the naphthalene and pentalene moieties, respectively (Figure 5). In any event, it looks like the ring currents in naphthalene-centered bispentalene **3** are much more localized than in benzo-centered bispentalenes **1** and **2**. Further investigations on the NICS-XY-scan of **S10**, a topologic isomer of **3**, and natural resonance theory (NRT) analysis of these two isomers suggest that **3** is better viewed as separate pentalenic and naphthalenic units (for further details, see Section S6.3, Supporting Information). The less reduced local paratropic ring current of the pentalene moieties, arising from the reduced delocalization with the adjacent naphthalene ring, might lead to the upfield shifts of proton H1 of **3b** compared to the corresponding resonances of **1b** and **2b**, which are observed by ^{1}H NMR spectroscopy (Figure 3).

Above all, NICS-XY-scans suggest a global paratropic current in the 18 π electron perimeter and a local diatropic current at the central six-membered ring for bispentalenes **1** and **2**, characteristic for antiaromaticity, while the 22 π-electron systems **3** showed more electron localization compared to **1** and **2**, with stronger paratropic ring currents on the pentalene moieties and diatropic current at the naphthalene moiety (Figure 5).

X-ray Crystallographic Analyses. Single crystals suitable for X-ray diffraction were grown by slow evaporation of $CHCl_3$/hexane (**2a**, for X-ray crystal structure, see Section S7.2, Supporting Information), $CDCl_3$ (**2b**), and CH_2Cl_2 (**3b**).

Views of the ORTEP drawings of bispentalenes **2b** and **3b** as well as the relevant bond lengths of the cores are shown in Figure 6. The crystal structures of both **2b** and **3b** show significant double- and single-bond alternation in the pentalene units, characteristic for antiaromaticity, similar to that of monobenzopentalene **S11**[23a] (Figure S50, Supporting Information). The degree of bond length alternation in **3b** and **S11** is slightly enhanced compared to that in **2b**. It is noteworthy that the length of a C−C bond in the pentalene moieties of **2b** and **3b** (around 1.50 Å, Figure 6a,c) is even longer than the expected bond length (1.48 Å) for a C(sp^2)−C(sp^2) single bond.[31] On the other hand, the alternation of bond lengths in the central six-membered rings is less pronounced pointing to a rather aromatic character.[31] These bond length alternations as well as the ^{1}H NMR chemical shifts indicate that the electron delocalization in the fused bispentalene cores of **2** and **3** is significantly decreased, compared to benzo-type aromatic systems. Although informative for the understanding of the global molecular properties, examination of only the fragmentary structures without considering the π-conjugated scaffold as a whole could be misleading. Therefore, average bond lengths of the entire chromophoric skeleton were calculated for **2b** (1.418 Å) and **3b** (1.421 Å), which are slightly larger than that of monobenzopentalene **S11** (1.415 Å).[23a]

Similar to **S11**,[23a] the bispentalene cores of **2b**, and **3b** are also planar with slight distortion. The aryl substituents are all twisted with different dihedral angles relative to the

DOI: 10.1021/jacs.5b03074
J. Am. Chem. Soc. 2015, 137, 7178−7188

bispentalene cores. The largest dihedral angle is much smaller for **2a** (43°) (Figure S47, Supporting Information) and **2b** (48°, phenyl rings on C(3), C(8), Figure 6b) than for **3b** (81°, phenyl rings on C(4), C(10), Figure 6d). These observations support the hypothesis for the stronger shielding effects on protons H2 and H3 in **3b** (Figure 3c).

The crystal packing of bispentalene derivative **3b** in the solid state was also investigated. As shown in Figure 7a, each molecule is connected to adjacent molecules in the same plane through C−H···π interactions with a distance d(C···π) of 3.507 Å (a). Furthermore, each molecule is tightly interlaced by four other molecules in two adjacent layers, and the structure is packed together by several C−H···π interactions (b−e) with distances d(C···π) between 3.416 and 3.589 Å. By virtue of these multiple weak noncovalent interactions, compound **3b** self-assembles into a layered structure (Figure 7b) in the solid state, with CH_2Cl_2 located in the interlayer space.

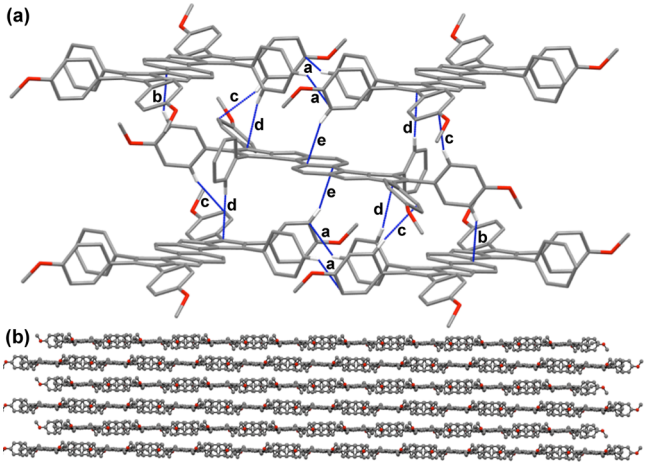

Figure 7. X-ray crystal structure of bispentalene **3b**. (a) View of the noncovalent interactions (dotted blue lines) between the adjacent molecules. Intermolecular distances (d(C···π): a: 3.507 Å; b: 3.418 Å; c: 3.544 Å; d: 3.589 Å; e: 3.416 Å. d(H···π): a: 2.737 Å; b: 2.631 Å; c: 2.595 Å; d: 2.752 Å; e: 2.628 Å). (b) View of the 3D layered structures; hydrogen atoms and solvent molecules (CH_2Cl_2) are omitted for clarity.

Optoelectronic Properties. The optoelectronic properties of bispentalene derivatives **1**−**3** were investigated by UV−vis absorption spectroscopy, TD-DFT calculations, as well as cyclic voltammetry (CV) and rotating disc voltammetry (RDV). The results are summarized in Table 1 (for full data set, see Section S9, Supporting Information).

The new compounds show specific colors in solution of CH_2Cl_2 or $CHCl_3$: compounds in series **1** are purple, those in series **2** pink, and those in series **3** orange (Figure S51, Supporting Information). These colors originate from intense absorptions in the Vis region. The UV−vis absorption spectra of bispentalenes **1**−**3** in $CHCl_3$ at 298 K are depicted in Figure 8.

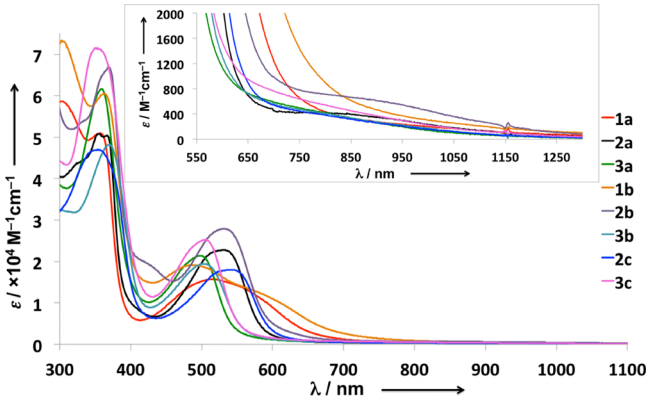

Figure 8. UV−vis spectra of bispentalene derivatives **1**, **2**, and **3** recorded at 298 K in $CHCl_3$ solution (4×10^{-5} M). Inset: long-wavelength, lowest-intensity absorptions corresponding to the symmetry-forbidden HOMO−LUMO transitions.

All compounds exhibited distinct absorptions in the 450−580 nm region with absorption coefficients (ε) reaching 2.5×10^4 M^{-1} cm^{-1}. Different from bispentalenes **2** and **3**, compounds **1a,b** displayed broad shoulders in the region of 550−700 nm. Most interestingly, all compounds feature weak, broad low-energy absorptions, which extend into the near-infrared region of the spectra and end beyond 1300 nm (0.95 eV). These absorptions represent HOMO−LUMO transitions,

Table 1. Computational, Electrochemical, and Optical Data for Bispentalene Derivatives 1−3

	calc[a]	electrochemical[b]						optical[e]	
comp.	E_{gap} ($S_0 \rightarrow S_1$) [eV]	E_{1ox}[c] [V]	E_{1red} [V]	E_{HOMO} [eV]	E_{LUMO} [eV]	E_{gap} [eV]	λ_{max} [nm]	λ_{max} [nm]	E_{gap} [eV]
1a	1.59	+0.25	−1.23[d]	−5.05	−3.57	1.48	838	–	–
1b	1.56	+0.12	−1.32[d]	−4.92	−3.48	1.44	861	–	–
2a	1.59	+0.25	−1.25[c]	−5.05	−3.55	1.50	827	820	1.51
2b	1.57	+0.15	−1.25[c]	−4.95	−3.55	1.40	885	885	1.40
2c	1.59	+0.48	−1.07[c]	−5.28	−3.73	1.55	800	790	1.57
3a	1.63	+0.27	−1.35[c]	−5.07	−3.45	1.62	765	770	1.61
3b	1.62	+0.20	−1.33[c]	−5.00	−3.47	1.53	810	801	1.55
3c	1.62	+0.47	−1.10[c]	−5.27	−3.70	1.57	790	772	1.61

[a]Calculations were performed at the CAM-B3LYP/6-31G(d)//ωB97X-D/6-31G(d) level of theory with chloroform solvation (PCM). [b]Electrochemical data obtained at a scan rate of 0.1 V s^{-1} in CH_2Cl_2 containing 0.1 M nBu$_4$NPF$_6$ on a glassy carbon working electrode. All potentials are given versus the Fc^+/Fc couple used as internal standard. HOMO and LUMO energy levels in eV were approximated from the reversible half-potential reduction waves or the irreversible first reduction wave using the equation, HOMO = −(4.80 + E_{1ox}), LUMO = −(4.80 + E_{1red}),[33] E_{gap} = LUMO − HOMO. λ_{max} is the calculated optical gap from redox data (λ_{max} = 1240/E_{gap}).[13d] [c]Reversible first reduction or oxidation wave. [d]Irreversible first reduction or oxidation wave. [e]The optical gap, E_{gap}, is defined as the energy corresponding to the lowest-energy absorption and estimated from corresponding spectra (E_{gap} = 1240/λ_{max}).[13d]

DOI: 10.1021/jacs.5b03074
J. Am. Chem. Soc. 2015, 137, 7178−7188

which are symmetry-forbidden as confirmed by time-dependent DFT calculations.

Clear differences between their low-energy absorptions could be seen for bispentalene derivatives with different central ring fusion. The lowest-intensity absorption of bispentalene **2a** with a central benzene ring appears at λ_{max} = 820 nm (1.51 eV, ε = 380 M^{-1} cm^{-1}), whereas for **3a** with the central naphthalene moiety, λ_{max} is observed around 770 nm (1.61 eV, ε = 400 M^{-1} cm^{-1}). The differences might be due to the reduced delocalization between the electronically more isolated pentalenic and naphthalenic units of **3a**, as confirmed through natural resonance theory analysis (NRT) (for further details, see Section S6.2, Supporting Information). Furthermore, the near orthogonal orientation between the peripheral phenyl rings and the bispentalene backbone in **3a** reduces the conjugation path length. No clear low-energy absorption maximum was observed for the U-shaped bispentalene **1a**,**b**. It might be overlapping with the broad shoulder peak covering the region of 550−700 nm.

The influence of the functional groups at the peripheral rings on the optical properties in **1**−**3** seems negligible. Comparison of the UV−vis spectra (Figure S52, Supporting Information) of unsubstituted **2a**, methoxy-substituted **2b**, and cyano-substituted **2c** revealed that only small shifts of the low-energy absorptions were observed. For compound **2b** with electron-donating methoxy-groups, a slight bathochromic shift of approximately 65 nm, whereas for **2c** with electron-withdrawing cyano groups, a hypsochromic shift of about 30 nm was detected. In agreement with the results from ^{1}H NMR spectroscopy, this suggests that the molecular properties of bispentalenes **1**−**3** are dominated by the conjugated core and not significantly influenced by the functional groups on the peripheral rings.

Calculations of the excited-state electronic properties of compounds **1**−**3** were performed by TD-DFT at the CAM-B3LYP/6-31G(d) level of theory using the software package Gaussian 09.[32a] In all cases, the computed transition energies are slightly larger than the experimental values with differences in the range of 0.03−0.12 eV for the lowest energy transition $S_0 \rightarrow S_1$, well within the expected error of recent benchmarks on common TD-DFT methods.[32b] These HOMO → LUMO transitions are symmetry-forbidden, as they would conserve symmetry with respect to an inversion center of the pentalene unit, which is reflected by the very low calculated oscillator strength f (typically f < 0.01). The second excited states all consist of a ∼ 1:1 composition of both HOMO−1 → LUMO and HOMO → LUMO+1 transitions, resulting in a similarly low-intense optical absorption band for the bispentalenes **2** and **3** (f < 0.001, each), because the HOMO → LUMO+1 vertical transition is symmetry-forbidden as revealed by TD-DFT calculations (Figure 9), whereas slightly higher oscillator strengths of 0.07 and 0.08 for **1a** and **1b** correspond to the broad shoulders that were observed in the absorption spectra at ca. 600 nm.

Trends in the properties in the series of bispentalenes **1**−**3** can be well predicted by TD-DFT calculations. The calculated energetic sequence of the lowest-energy absorption of **1a** ≈ **2a** < **3a** is in good agreement with the experimental UV−vis spectra (Figure 8 and Section S8, Supporting Information) and electrochemical results. Similarly reproduced is the trend of the third excitation state in the energetic sequence **1** ≈ **3** > **2**, all showing intense oscillator strength of f > 0.5, in agreement with the absorptions around 500 nm.

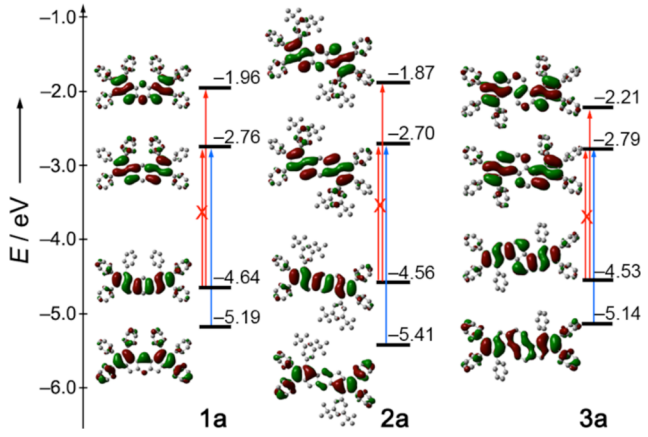

Figure 9. Calculated (B3LYP/6-31G(d)) orbital energy diagram of HOMO−1, HOMO, LUMO, and LUMO+1 for bispentalenes **1a**, **2a**, and **3a**. Red and blue arrows represent symmetry-forbidden and symmetry-allowed transitions, respectively.

By cyclic voltammetry, bispentalenes **1**−**3** commonly exhibit two reversible oxidation waves and two reversible reduction waves in CH_2Cl_2 at 298 K (vs Fc^+/Fc, + 0.1 M nBu$_4$NPF$_6$; for detailed cyclic voltammogramms, linear sweep voltammogramms or redox potentials, see Section S9, Supporting Information). For example in compounds **2a** and **3b**, the first reversible oxidation occurs at +0.25 V and +0.20 V, while reduction occurs at −1.25 and −1.33 V, respectively. Compounds **1b** and **3c**, however, showed a first irreversible reduction peak and a second reversible electron transfer. In contrast, the first reduction for bispentalene **1a** was reversible whereas a second step presented an irreversible reduction peak. Substitution effects are as expected: methoxy groups shifts the first oxidation potential to more negative values, whereas cyano substitution leads to anodic shifts of first reduction potentials. On the basis of the experimental values, LUMO energy levels for **1a**, **2a**, and **3a** are estimated as −3.57, −3.55, and −3.45 eV, respectively, while all HOMO energy levels are maintained at around the same value of −5.05 eV. Interestingly, π-electron extension only raises the LUMO energy levels and has no obvious effects on the HOMO energy levels in these series of polycyclic hydrocarbons. The higher LUMO energy level of **3a** signifies that the naphthalene-fused bispentalene is less easily reduced than benzene-fused **1a** and **2a**, suggesting a stronger coupling across the π-framework of **1** and **2**. Furthermore, the same HOMO energy level indicates that the extension of the π-system has almost no effect on the oxidation properties in these series or the effect is balanced by some other factors. These energy levels lead to HOMO−LUMO energy gap of 1.48, 1.50, and 1.62 eV for **1a**, **2a**, and **3a**, respectively, in agreement with the optical gaps calculated from the lowest-energy in the UV−vis spectra.

The small effect of the functional groups on the peripheral phenyl rings is also reflected by the values of HOMO−LUMO gaps (Table 1). Bispentalene derivative **2b** has the lowest HOMO−LUMO energy gap of 1.40 eV, and this value is lower than in other neutral, π-conjugated polycyclic hydrocarbons containing the same number of fused rings. The same value was obtained for unsubstituted hexacene in a thin film, which is thermally stable in the solid state in dark, but highly unstable in solutions or when exposed to light.[34] The electrochemical gaps are all in good agreement with the energy gaps derived from the absorption spectra, and calculated by the DFT methods.

DOI: 10.1021/jacs.5b03074
J. Am. Chem. Soc. 2015, 137, 7178−7188

SUMMARY AND CONCLUSIONS

Three series of stable, neutral, π-extended bispentalene derivatives with different fusion patterns and functional groups on the peripheral phenyl groups were synthesized by a modified double carbopalladation cascade reaction between acetylenes and bis(*gem*-dibromoolefins) with the formation of six C−C bonds during the one-pot reaction. Although the synthesized hydrocarbons have overall $[4n+2]$ π-electrons in the backbone, their ^{1}H NMR spectra showed intensive upfield shifts of the protons in the pentalene subunits, comparable to antiaromatic monobenzopentalene derivatives.[23a] Further investigations on the magnetic shielding properties were performed through NICS-XY-scans, suggesting for 18 π-electron systems **1** and **2** a global paratropic ring current and a local diatropic ring current at the central benzene ring. In contrast, ring currents in 22 π-electron bispentalene systems **3** with a central naphthalene moiety are found to be more localized compared to **1** and **2**. X-ray crystal structures of **2a**,**b** and **3b** revealed planar bispentalene cores with large double- and single-bond alternation in the pentalene subunits while much smaller bond alternation is seen in the central benzene or naphthalene rings. Compound **3b** was shown to self-assemble into a layered 3D structure in the solid state. Interestingly, the UV−vis spectra of the new compounds all exhibit broad, low-energy absorptions extending into the near-infrared region. In agreement with TD-DFT results, both optical and electrochemical data showed much smaller HOMO−LUMO energy gaps compared to other stable neutral acene-like conjugated hydrocarbons containing the same number of fused rings. The experimental results in combination with theoretical calculations are indicative of the overall antiaromatic character of bispentalenes **1**−**3** containing two 8 π-electron pentalene units in spite of their $[4n+2]$ π-electron perimeters. Because of its low HOMO−LUMO band gap, environmental stability and excellent solubility, bispentalene **2a** is a promising candidate for use in organic electronic devices.

The present study not only introduces new bispentalene-based chromophores, but also emphasizes the importance of local structures in global molecular properties. Thus, it is broadening the design strategies toward molecules with low-energy band gaps and higher stability for organic materials applications.

EXPERIMENTAL SECTION

General Procedure for the Synthesis of Bispentalene Derivatives via Carbopalladation Cascade Reaction. Bis(*gem*-dibromoolefin) (1.0 equiv), alkyne (6.0 equiv), $[Pd(PPh_3)_2Cl_2]$ (0.2 equiv), zinc dust (2.0 equiv), and K_2CO_3 (4.0 equiv) were placed in a dry Schlenk tube. The tube was evacuated and refilled with nitrogen five times. Dry toluene (enough to generate a 0.04 M solution of bis(*gem*-dibromoolefin)) was added, the tube was sealed, and the mixture stirred at 110 °C for 1−2 h, and then hydroquinone (4.0 equiv) was added. The reaction mixture was continued stirring at 110 °C for another 24 h. After evaporation, the residue was purified by column chromatography. The excess of the alkyne could be recovered after the chromatographic separation by recrystallization.

1,2,6,7-Tetrakis(4-methoxyphenyl)-3,5-diphenyldicyclopenta[*a*,*h*]-*s*-indacene 1b. A mixture of **4** (50 mg, 0.08 mmol), **5b** (111 mg, 0.47 mmol), $[Pd(PPh_3)_2Cl_2]$ (11 mg, 0.02 mmol), K_2CO_3 (43 mg, 0.32 mmol), Zn dust (11 mg, 0.16 mmol), and hydroquinone (34 mg, 0.32 mmol) in toluene (2 mL) was treated according to the general procedure to give **1b** (13 mg, 21%) as a dark-purple solid. Column chromatography (Alumina N; hexane/CH_2Cl_2 1:2): Dec. > 250 °C; R_f = 0.30 (Alumina B; cyclohexane/CH_2Cl_2 1:2); ^{1}H NMR (400 MHz, $CDCl_3$) δ = 3.74 (s, 6H, 2 OCH_3), 3.76 (s, 6H, 2 OCH_3), 6.05 (s, 2H, H−C(8,10)), 6.13 (s, 1H, H−C(4)), 6.46 (s, 1H, H−C(9)), 6.63 (d, J = 8.8 Hz, 4H, arom.), 6.71 (d, J = 8.9 Hz, 4H, arom.), 6.74 (d, J = 8.8 Hz, 4H, arom.), 6.88−6.95 (m, 4H, arom.), 7.00 (d, J = 8.9 Hz, 4H, arom.), 7.05−7.09 (m, 4H, arom.), 7.14−7.23 (m, 2H, arom.) ppm; ^{13}C NMR (100 MHz, $CDCl_3$) δ = 55.05, 55.14, 113.14, 113.47, 114.67, 120.23, 127.21, 127.31, 127.80, 127.83, 128.93, 129.50, 130.77, 132.48, 133.07, 134.15, 137.22, 139.92, 145.28, 145.91, 147.54, 153.06, 158.46, 158.49 ppm; UV−vis ($CHCl_3$) λ_{max} (lgε) 367 (ca. 4.78), 492 (ca. 4.27), 608 (ca. 4.01) nm; HR-MALDI/ESI-MS m/z (%) 804.3136 (20), 803.3105 (63), 802.3074 (100, $[M]^+$, calcd for $C_{58}H_{42}O_4^+$: 802.3078).

3,8-Bis(3,5-di-*t*-butylphenyl)-1,2,6,7-tetrakis(4-methoxyphenyl)dicyclo-penta[*a*,*g*]-*s*-indacene 2b. A mixture of **6** (50 mg, 0.06 mmol), **5b** (82 mg, 0.36 mmol), $[Pd(PPh_3)_2Cl_2]$ (8 mg, 0.01 mmol), K_2CO_3 (32 mg, 0.24 mmol), Zn dust(8 mg, 0.12 mmol), and hydroquinone (25 mg, 0.24 mmol) in toluene (2 mL) was treated according to the general procedure to give **2b** (12 mg, 20%) as a black solid. Column chromatography (Alumina N; hexane/CH_2Cl_2 5:1): mp 263−264 °C; R_f = 0.28 (Alumina B; cyclohexane/CH_2Cl_2 1:1); ^{1}H NMR (400 MHz, $CDCl_3$) δ = 1.17 (s, 36H, 4 CMe_3), 3.73 (s, 6H, 2 OCH_3), 3.76 (s, 6H, 2 OCH_3), 5.92 (s, 2H, H−C(5,10)), 6.43 (s, 2H, H−C(4,9)), 6.68−6.75 (m, 14H, arom.), 6.85 (s, 4H, arom.), 6.99−7.02 (m, 4H, arom.) ppm; ^{13}C NMR (100 MHz, $CDCl_3$) δ = 31.27, 34.76, 55.21, 113.30, 113.50, 117.62, 121.86, 123.94, 127.27, 127.76, 129.50, 130.88, 132.11, 132.24, 132.90, 135.44, 139.06, 146.08, 146.23, 148.86, 149.52, 153.70, 158.41, 158.54 ppm; UV−vis ($CHCl_3$) λ_{max} (lgε) 370 (ca. 4.82), 535 (ca. 4.44), 885 (ca. 2.79) nm; HR-MALDI/ESI-MS m/z (%) 1028.5652 (32), 1027.5617 (79), 1026.5580 (100, $[M]^+$, calcd for $C_{74}H_{74}O_4^+$: 1026.5582).

2,3,8,9-Tetrakis(4-methoxyphenyl)-4,10-diphenyldipentaleno[1,2-*a*:1′,2′-*f*]-naphthalene 3b. A mixture of **7** (100 mg, 0.14 mmol), **5b** (205 mg, 0.84 mmol), $[Pd(PPh_3)_2Cl_2]$ (20 mg, 0.03 mmol), K_2CO_3 (80 mg, 0.56 mmol), Zn dust (19 mg, 0.28 mmol), and hydroquinone (63 mg, 0.56 mmol) in toluene (4 mL) was treated according to the general procedure to give **3b** (34 mg, 28%) as a brown solid. Column chromatography (Alumina N; hexane/CH_2Cl_2 4:1): mp 291−292 °C; R_f = 0.65 (Alumina B; CH_2Cl_2); ^{1}H NMR (400 MHz, $CDCl_3$) δ = 3.71 (s, 6H, 2 OCH_3), 3.75 (s, 6H, 2 OCH_3), 5.82 (s, 2H, H−C(1,7)), 5.93 (d, J = 8.2 Hz, 2H, H−C(5,11)), 6.02 (d, J = 8.4 Hz, 2H, H−C(6,12)), 6.57 (d, J = 8.9 Hz, 4H, arom.), 6.68 (2d, J = 8.9 Hz, 8H, arom.), 6.94 (d, J = 8.8 Hz, 4H, arom.), 7.01−7.09 (m, 4H, arom.), 7.17−7.25 (m, 6H, arom.) ppm; ^{13}C NMR (100 MHz, $CDCl_3$) δ = 55.03, 55.15, 113.08, 113.43, 122.10, 125.57, 126.64, 127.41, 128.05, 129.21, 129.31, 129.48, 130.55, 132.58, 133.48, 134.86, 135.52, 142.79, 146.11, 146.63, 148.71, 155.16, 158.42, 158.55 ppm UV−vis ($CHCl_3$) λ_{max} (lgε) 374 (ca. 4.68), 507 (ca. 4.29), 801 (ca. 2.59) nm; HR-MALDI/ESI-MS m/z (%) 854.3300 (23), 853.3269 (66), 852.3233 (100, $[M]^+$, calcd for $C_{62}H_{44}O_4^+$:852.3234).

ASSOCIATED CONTENT

Supporting Information

Materials and methods, experimental details and data for new compounds as well as copies of ^{1}H and ^{13}C NMR spectra for new compounds, X-ray crystallographic data and CIF files for **2a**, **2b**, and **3b**, full data set of UV−vis spectroscopy, cyclic voltammetry (CV) and rotating disc voltammetry (RDV) results, computational details for **1**, **2**, and **3**, and relative stabilities in solution. The Supporting Information is available free of charge on the ACS Publications website at DOI: 10.1021/jacs.5b03074.

AUTHOR INFORMATION

Corresponding Authors

*stanger@tx.technion.ac.il
*diederich@org.chem.ethz.ch

DOI: 10.1021/jacs.5b03074
J. Am. Chem. Soc. 2015, 137, 7178−7188

Present Address
[⊥]MTA-SZTE Stereochemistry Research Group, Dóm tér 8, Szeged 6720, Hungary.

Author Contributions
[∥]J.C., G. L., and O.D. contributed equally.

Notes
The authors declare no competing financial interest.

■ ACKNOWLEDGMENTS

This work was supported by a grant from the Swiss National Science Foundation (SNF). O.D. acknowledges support by a Kekulé fellowship (Fonds der Chemischen Industrie) and the Studienstiftung des Deutschen Volkes. A.S. thanks the Israel Science Foundation (ISF, Grant Number 1485/11) for financial support. In memory of Prof. Paul von Ragué Schleyer.

■ REFERENCES

(1) (a) Garratt, P. J. *Aromaticity*; John Wiley and Sons: New York, 1986. (b) Minkin, V. I.; Glukhovtsev, M. N.; Simkin, B. Y. *Aromaticity and Antiaromaticity*; John Wiley and Sons: New York, 1994. (c) Allen, A. D.; Tidwell, T. T. *Chem. Rev.* **2001**, *101*, 1333−1348. (d) Gomes, J. A. N. F.; Mallion, R. B. *Chem. Rev.* **2001**, *101*, 1349−1383. (e) Gleiter, R.; Haberhauer, G. *Aromaticity and Other Conjugation Effects*; Wiley-VCH: Weinheim, Germany, 2012.

(2) (a) Hückel, E. Z. *Z. Phys.* **1931**, *70*, 204−286. (b) Hückel, E. Z. *Z. Phys.* **1932**, *76*, 628−648. (c) Hückel, E. Z. *Z. Electrochem.* **1937**, *43*, 752−788.

(3) Frost, A. A.; Musulin, B. *J. Chem. Phys.* **1953**, *21*, 572−573.

(4) (a) Breslow, R. *Chem. Eng. News* **1965**, *43*, 90−100. (b) Breslow, R. *Acc. Chem. Res.* **1973**, *6*, 393−398.

(5) Krygowski, T. M.; Cyrañski, M. K.; Czarnocki, Z.; Häfelinger, G.; Katritzky, A. R. *Tetrahedron* **2000**, *56*, 1783−1796.

(6) For some examples, see: (a) Schleyer, P. v. R.; Jiao, H. *Pure Appl. Chem.* **1996**, *68*, 209−218. (b) Cyrañski, M. K.; Krygowski, T. M.; Katritzky, A. R.; Schleyer, P. v. R. *J. Org. Chem.* **2002**, *67*, 1333−1338. (c) Stanger, A. *Chem. Commun.* **2009**, 1939−1947.

(7) For some examples, see: (a) Zahradnik, R. *Angew. Chem., Int. Ed.* **1965**, *4*, 1039−1050. (b) Bochvar, D. A.; Gal'pern, E. G.; Gambaryan, N. P. *Bull. Acad. Sci. USSR, Div. Chem. Sci.* **1970**, *19*, 377−379. (c) Randić, M. *J. Am. Chem. Soc.* **1977**, *99*, 444−450. (d) Randić, M. *Chem. Rev.* **2003**, *103*, 3449−3605.

(8) Stowasser, B.; Hafner, K. *Angew. Chem., Int. Ed. Engl.* **1986**, *25*, 466−468.

(9) For some recent examples, see: (a) Hoheisel, T. N.; Schrettl, S.; Szilluweit, R.; Frauenrath, H. *Angew. Chem., Int. Ed.* **2010**, *49*, 6496−6515. (b) Pisula, W.; Feng, X.; Müllen, K. *Chem. Mater.* **2011**, *23*, 554−567. (c) Figueira-Duarte, T. M.; Müllen, K. *Chem. Rev.* **2011**, *111*, 7260−7314. (d) Henson, Z. B.; Müllen, K.; Bazan, G. C. *Nat. Chem.* **2012**, *4*, 699−704.

(10) For some recent reviews, see: (a) Wang, C.; Dong, H.; Hu, W.; Liu, Y.; Zhu, D. *Chem. Rev.* **2012**, *112*, 2208−2267. (b) Mei, J.; Diao, Y.; Appleton, A. L.; Fang, L.; Bao, Z. *J. Am. Chem. Soc.* **2013**, *135*, 6724−6746.

(11) For some examples, see: (a) Coppo, P.; Yeates, S. G. *Adv. Mater.* **2005**, *17*, 3001−3005. (b) Anthony, J. E. *Chem. Rev.* **2006**, *106*, 5028−5048. (c) Palayangoda, S. S.; Mondal, R.; Shah, B. K.; Neckers, D. C. *J. Org. Chem.* **2007**, *72*, 6584−6587. (d) Anthony, J. E. *Angew. Chem., Int. Ed.* **2008**, *47*, 452−483. (e) Kaur, I.; Jia, W.; Kopreski, R. P.; Selvarasah, S.; Dokmeci, M. R.; Pramanik, C.; McGruer, N. E.; Miller, G. P. *J. Am. Chem. Soc.* **2008**, *130*, 16274−16286.

(12) (a) Breslow, R.; Foss, F. W., Jr. *J. Phys.: Condens. Matter* **2008**, *20*, 374104. (b) Breslow, R.; Schneebeli, S. T. *Tetrahedron* **2011**, *67*, 10171−10178.

(13) For some recent examples, see: (a) Pho, T. V.; Yuen, J. D.; Kurzman, J. A.; Smith, B. G.; Miao, M.; Walker, W. T.; Seshadri, R.; Wudl, F. *J. Am. Chem. Soc.* **2012**, *134*, 18185−18188. (b) Bunz, U. H. F.; Engelhart, J. U.; Lindner, B. D.; Schaffroth, M. *Angew. Chem., Int. Ed.* **2013**, *52*, 3810−3821. (c) Jiang, W.; Li, Y.; Wang, Z. *Chem. Soc. Rev.* **2013**, *42*, 6113−6127. (d) Yue, W.; Suraru, S.-L.; Bialas, D.; Müller, M.; Würthner, F. *Angew. Chem., Int. Ed.* **2014**, *53*, 6159−6162. (e) Engelhart, J. U.; Tverskoy, O.; Bunz, U. H. F. *J. Am. Chem. Soc.* **2014**, *136*, 15166−15169.

(14) For some recent examples of conjugated PAHs containing seven- and eight-membered rings, see: (a) Feng, C.-N.; Kuo, M.-Y.; Wu, Y.-T. *Angew. Chem., Int. Ed.* **2013**, *52*, 7791−7794. (b) Yang, X.; Liu, D.; Miao, Q. *Angew. Chem., Int. Ed.* **2014**, *53*, 6786−6790.

(15) For some recent examples of fully π-conjugated indenofluorene systems, see: (a) Chase, D. T.; Rose, B. D.; McClintock, S. P.; Zakharov, L. N.; Haley, M. M. *Angew. Chem., Int. Ed.* **2011**, *50*, 1127−1130. (b) Chase, D. T.; Fix, A. G.; Kang, S. J.; Rose, B. D.; Weber, C. D.; Zhong, Y.; Zakharov, L. N.; Lonergan, M. C.; Nuckolls, C.; Haley, M. M. *J. Am. Chem. Soc.* **2012**, *134*, 10349−10352. (c) Nishida, J.; Tsukaguchi, S.; Yamashita, Y. *Chem.—Eur. J.* **2012**, *18*, 8964−8970. (d) Fix, A. G.; Deal, P. E.; Vonnegut, C. L.; Rose, B. D.; Zakharov, L. N.; Haley, M. M. *Org. Lett.* **2013**, *15*, 1362−1365. (e) Shimizu, A.; Kishi, R.; Nakano, M.; Shiomi, D.; Sato, K.; Takui, T.; Hisaki, I.; Miyata, M.; Tobe, Y. *Angew. Chem., Int. Ed.* **2013**, *52*, 6076−6079. (f) Tobe, Y. *Chem. Rec.* **2015**, *15*, 86−96.

(16) (a) Müller, E.; Fritz, H.-G.; Munk, K.; Straub, H.; Geisel, M. v. H. *Tetrahedron Lett.* **1969**, *10*, 5167−5170. (b) Scherf, U.; Müllen, K. *Polymer* **1992**, *33*, 2443−2446. (c) Levi, Z. U.; Tilley, T. D. *J. Am. Chem. Soc.* **2010**, *132*, 11012−11014.

(17) (a) Bally, T.; Chai, S.; Neuenschwander, M.; Zhu, Z. *J. Am. Chem. Soc.* **1997**, *119*, 1869−1875. (b) Fowler, P. W.; Soncini, A. *Polycyclic Aromat. Compd.* **2004**, *24*, 353−366. (c) Cuesta, I. G.; Ligabue, A.; Sánchez de Merás, A.; Lazzeretti, P. *Chem. Phys. Lett.* **2005**, *401*, 282−287.

(18) (a) Le Goff, E. *J. Am. Chem. Soc.* **1962**, *84*, 3975−3976. (b) Hafner, K.; Bangert, K. F.; Orfanos, V. *Angew. Chem., Int. Ed.* **1967**, *6*, 451−452. (c) Hafner, K.; Süss, H. U. *Angew. Chem., Int. Ed.* **1973**, *12*, 575−577. (d) Hafner, K.; Suda, M. *Angew. Chem., Int. Ed. Engl.* **1976**, *15*, 314−315. (e) Hafner, K.; Goltz, M. *Angew. Chem., Int. Ed. Engl.* **1982**, *21*, 695−696.

(19) For some recent examples, see: (a) Kawase, T.; Fujiwara, T.; Kitamura, C.; Konishi, A.; Hirao, Y.; Matsumoto, K.; Kurata, H.; Kubo, T.; Shinamura, S.; Mori, H.; Miyazaki, E.; Takimiya, K. *Angew. Chem., Int. Ed.* **2010**, *49*, 7728−7732. (b) Hashmi, A.; Stephen, K.; Wieteck, M.; Braun, I.; Nösel, P.; Jongbloed, L.; Rudolph, M.; Rominger, F. *Adv. Synth. Catal.* **2012**, *354*, 555−562. (c) Maekawa, T.; Segawa, Y.; Itami, K. *Chem. Sci.* **2013**, *4*, 2369−2373. (d) Zhao, J.; Oniwa, K.; Asao, N.; Yamamoto, Y.; Jin, T. *J. Am. Chem. Soc.* **2013**, *135*, 10222−10225. (e) Shen, J.; Yuan, D.; Qiao, Y.; Shen, X.; Zhang, Z.; Zhong, Y.; Yi, Y.; Zhu, X. *Org. Lett.* **2014**, *16*, 4924−4927. (f) Nakano, M.; Osaka, I.; Takimiya, K. *J. Mater. Chem. C* **2015**, *3*, 283−290. (g) Dai, G.; Chang, J.; Zhang, W.; Bai, S.; Huang, K.-W.; Xu, J.; Chi, C. *Chem. Commun.* **2015**, *51*, 503−506.

(20) (a) Chen, C.; Harhausen, M.; Liedtke, R.; Bussmann, K.; Fukazawa, A.; Yamaguchi, S.; Petersen, J. L.; Daniliuc, C. G.; Fröhlich, R.; Kehr, G.; Erker, G. *Angew. Chem., Int. Ed.* **2013**, *52*, 5992−5996. (b) Chen, C.; Harhausen, M.; Fukazawa, A.; Yamaguchi, S.; Fröhlich, R.; Daniliuc, C. G.; Petersen, J. L.; Kehr, G.; Erker, G. *Chem.—Asian J.* **2014**, *9*, 1671−1681.

(21) For some recent examples, see: (a) Zhang, H.; Karasawa, T.; Yamada, H.; Wakamiya, A.; Yamaguchi, S. *Org. Lett.* **2009**, *11*, 3076−3079. (b) Saito, M.; Hashimoto, Y.; Tajima, T.; Ishimura, K.; Nagase, S.; Minoura, M. *Chem.—Asian J.* **2012**, *7*, 480−483. (c) Xu, F.; Peng, L.; Orita, A.; Otera, J. *Org. Lett.* **2012**, *14*, 3970−3973.

(22) Nakano, M.; Osaka, I.; Takimiya, K.; Koganezawa, T. *J. Mater. Chem. C* **2014**, *2*, 64−70.

(23) (a) Rivera-Fuentes, P.; von Wantoch Rekowski, M.; Schweizer, W. B.; Gisselbrecht, J.-P.; Boudon, C.; Diederich, F. *Org. Lett.* **2012**, *14*, 4066−4069. (b) London, G.; von Wantoch Rekowski, M.; Dumele, O.; Schweizer, W. B.; Gisselbrecht, J.-P.; Boudon, C.; Diederich, F. *Chem. Sci.* **2014**, *5*, 965−972.

(24) Gershoni-Poranne, R.; Stanger, A. *Chem.—Eur. J.* **2014**, *20*, 5673−5688.

DOI: 10.1021/jacs.5b03074
J. Am. Chem. Soc. 2015, 137, 7178−7188

(25) Chelucci, G. *Chem. Rev.* **2012**, *112*, 1344−1462.
(26) Pople, J. A.; Untch, K. G. *J. Am. Chem. Soc.* **1966**, *88*, 4811−4815.
(27) Dauben, H. J., Jr.; Wilson, J. D.; Laity, J. L. *J. Am. Chem. Soc.* **1968**, *90*, 811−813.
(28) (a) Schleyer, P. v. R.; Maerker, C.; Dransfeld, A.; Jiao, H.; van Eikema Hommes, N. J. R. *J. Am. Chem. Soc.* **1996**, *118*, 6317−6318. (b) Chen, Z.; Wannere, C. S.; Corminboeuf, C.; Puchta, R.; Schleyer, P. v. R. *Chem. Rev.* **2005**, *105*, 3842−3888.
(29) (a) Bultinck, P. *Faraday Discuss.* **2007**, *135*, 347−365. (b) Schleyer, P. v. R.; Wu, J. I.; Cossío, F. P.; Fernández, I. *Chem. Soc. Rev.* **2014**, *43*, 4909−4921.
(30) Ring current of *X* ppm means an induced ring current that produces an induced magnetic field which give rise to NICS(1.7)$_{\pi,ZZ}$ of *X* ppm. This terminology is used from now on when quantitative comparisons are wished.
(31) Smith, M. B.; March, J. *March's Advanced Organic Chemistry*, 6th ed.; John Wiley & Sons: New York, 2007; Chapters 1 and 2, pp 3−105.
(32) (a) Frisch, M. J.; Trucks, G. W.; Schlegel, H. B.; Scuseria, G. E.; Robb, M. A.; Cheeseman, J. R.; Scalmani, G.; Barone, V.; Mennucci, B.; Petersson, G. A.; Nakatsuji, H.; Caricato, M.; Li, X.; Hratchian, H. P.; Izmaylov, A. F.; Bloino, J.; Zheng, G.; Sonnenberg, J. L.; Hada, M.; Ehara, M.; Toyota, K.; Fukuda, R.; Hasegawa, J.; Ishida, M.; Nakajima, T.; Honda, Y.; Kitao, O.; Nakai, H.; Vreven, T.; Montgomery, J. A., Jr.; Peralta, J. E.; Ogliaro, F.; Bearpark, M.; Heyd, J. J.; Brothers, E.; Kudin, K. N.; Staroverov, V. N.; Kobayashi, R.; Normand, J.; Raghavachari, K.; Rendell, A.; Burant, J. C.; Iyengar, S. S.; Tomasi, J.; Cossi, M.; Rega, N.; Millam, M. J.; Klene, M.; Knox, J. E.; Cross, J. B.; Bakken, V.; Adamo, C.; Jaramillo, J.; Gomperts, R.; Stratmann, R. E.; Yazyev, O.; Austin, A. J.; Cammi, R.; Pomelli, C.; Ochterski, J. W.; Martin, R. L.; Morokuma, K.; Zakrzewski, V. G.; Voth, G. A.; Salvador, P.; Dannenberg, J. J.; Dapprich, S.; Daniels, A. D.; Farkas, Ö.; Foresman, J. B.; Ortiz, J. V.; Cioslowski, J.; Fox, D. J. *Gaussian 09*, Revision D.01; Gaussian, Inc.: Wallingford, CT, 2013. (b) Laurent, A. D.; Jacquemin, D. *Int. J. Quantum Chem.* **2013**, *113*, 2019−2039.
(33) (a) Pommerehne, J.; Vestweber, H.; Guss, W.; Mahrt, R. F.; Bässler, H.; Porsch, M.; Daub, J. *Adv. Mater.* **1995**, *7*, 551−554. (b) D'Andrade, B. W.; Datta, S.; Forrest, S. R.; Djurovich, P.; Polikarpov, E.; Thompson, M. E. *Org. Electron.* **2005**, *6*, 11−20.
(34) Watanabe, M.; Chang, Y. J.; Liu, S.-W.; Chao, T.-H.; Goto, K.; Islam, M. M.; Yuan, C.-H.; Tao, Y.-H.; Shinmyozu, T.; Chow, T. J. *Nat. Chem.* **2012**, *4*, 574−578.

DOI: 10.1021/jacs.5b03074
J. Am. Chem. Soc. 2015, 137, 7178−7188